 https://doi.org/10.3311/PPci.40312 Creative Commons Attribution

Periodica Polytechnica Civil Engineering, 69(4), pp. 1298–1310, 2025

Parametric Study on the Effect of Axial Force on the Seismic Performance of the Bar Damper

Kambiz Cheraghi[1*], Zeinab Kahrari[1], Mohammad Hadi Tavana[2]

[1] Department of Civil Engineering, Faculty of Engineering, Razi University, Kermanshah 6714473421, Iran
[2] Department of Civil Engineering, Ker.C., Islamic Azad University, Kermanshah, 6714414971, Iran
[*] Corresponding author, e-mail: kambiz.cheraghi@gmail.com

Received: 26 February 2025, Accepted: 30 September 2025, Published online: 18 October 2025

Abstract

A bar damper (BD) is an energy-absorbing device that, despite its simplicity, exhibits excellent energy absorption capacity. The parametric studies in this research focused on the effect of axial force on the cyclic behavior of these dampers. Initially, to verify the results of the numerical model, three experimental BD samples with different heights were utilized. After calculating the buckling load of BD, the effect of 2% and 4% of this load on its cyclic behavior was investigated. The effect of axial force and damper dimensions on its seismic parameters was assessed through nonlinear static analyses. These parameters included initial and effective stiffness, strength, energy dissipation, and equivalent damping ratio (EDR). Additionally, based on the curve fitting method for estimating the initial stiffness of the damper under axial force, an approximate equation was provided, which showed acceptable accuracy compared to the numerical results. The results indicated that the axial force led to a reduction in elastic stiffness, effective stiffness, and strength of the damper, especially at large deformations. The impact on energy dissipation was negligible, but it caused an increase in the EDR. The greatest impact of the axial force was observed on the strength, followed by its effect on the EDR.

Keywords

bar damper, axial force, energy dissipation, hysteretic behavior, numerical analysis, metallic passive dampers

1 Introduction

In conventional structures, the dissipation of seismic input energy is achieved through the elasto-plastic behavior of structural elements. However, this approach can result in significant residual deformations after major seismic events [1, 2]. To mitigate this problem, passive control strategies have been implemented [3, 4]. Central to these strategies is the design of dampers, which play a crucial role during earthquakes by dissipating the seismic energy introduced into the structure. As a result, the primary structure remains largely undamaged, and the focus of damage is shifted to the dampers, which can be conveniently replaced following intense seismic activity [5, 6]. Dampers are generally categorized based on their energy dissipation mechanisms, including metal dampers [7, 8], viscoelastic dampers, friction dampers [9], viscous dampers [10], and smart dampers. Among these, metal dampers are particularly favored due to their straightforward mechanical modeling and excellent energy dissipation capabilities [11].

Many yield dampers with different geometries and functions have been proposed in past research. Shahri and Mousavi [12] investigated the use of steel slit dampers in beam-to-column connections to improve seismic performance and prevent brittle failure. They proposed elliptic slit dampers, which enhance energy dissipation and reduce stress concentration at strut ends. Parametric analysis revealed that these dampers contributed about 97.19% to energy dissipation, significantly improving the connections' overall seismic resilience. Lotfi Mahyari et al. [13] introduced a novel yielding damper with a pure torsional mechanism, maximizing energy dissipation by eliminating shear force and bending moment. Analytical relationships for structural characteristics were derived, and ten specimens tested under cyclic loading showed stable hysteresis, high energy absorption, and ductility. Equivalent viscous damping ratios ranged from 38% to 48%, aligning well with analytical predictions. Gorji Azandariani et al. [14] introduced the energy absorption system of a steel dual-ring damper and analyzed its cyclic behavior analytically and numerically. They derived relationships for yield strength, yield displacement, and elastic stiffness, validated through

Cite this article as: Cheraghi, K., Kahrari, Z., Tavana, M. H. "Parametric Study on the Effect of Axial Force on the Seismic Performance of the Bar Damper", Periodica Polytechnica Civil Engineering, 69(4), pp. 1298–1310, 2025. https://doi.org/10.3311/PPci.40312

parametric studies and finite element models. Results showed increased energy dissipation with larger ring diameters, while higher diameter-to-thickness ratios reduced ductility and damping. Ghamari et al. [15] addressed the limitations of concentrically braced frames, such as low ductility and poor energy dissipation, by introducing an I-shaped steel damper with a shear yield mechanism. This economical and easily replaceable damper prevents diagonal brace buckling, acting as a ductile fuse. Numerical and parametric analyses confirmed its effectiveness, with overstrength exceeding 1.5, as recommended by AISC. Zhou et al. [16] introduced a novel double C-section steel slit damper, conducting six cyclic loading tests to assess the effects of strip aspect ratio, flange thickness, damper length, and steel grades on its hysteretic behavior and resistance. The damper demonstrated strong structural performance, with numerical models confirming experimental results. However, existing design equations yielded inconsistent initial stiffness predictions and conservative ultimate strength estimates. Yang et al. [17] introduced a shear-bending metallic damper with a double-phased yield mechanism, optimizing energy dissipation and stiffness by combining bending and shear plates. Testing ten specimens revealed satisfactory plastic development, strong energy dissipation, and good ductility, with two identified failure modes. Parameter analysis confirmed the mechanism's effectiveness, and potential improvements were suggested to prevent premature weld failures. Qiu et al. [18] addressed the limitations of traditional U-shaped dampers by developing a new T-section metallic damper. Theoretical and experimental studies evaluated the seismic performance, with derived formulas for yield strength and initial stiffness showing higher stiffness, strength, and energy dissipation than U-shaped dampers. Numerical simulations quantified the impact of geometry and materials, highlighting enhanced performance with shape memory alloys. In other studies, the seismic behavior of U-shaped [19–22], box-shaped [23], S-shaped [24–26], and X-shaped dampers [26, 27] has also been investigated. In these studies, important seismic parameters of the dampers, including elastic stiffness, yield force, ultimate strength, and energy absorption, have been investigated.

Ghaedi et al. [28] introduce a novel yielding damper known as the Bar Damper (BD), which consists of solid bars sandwiched between two plates. The study formulates design parameters through simplified mechanical modeling, demonstrating that the device exhibits stable hysteretic behavior under cyclic loading. The Bar Damper maintains significant displacement capacity with minimal degradation in strength and stiffness. The slenderness ratio of the bars is identified as a key design factor influencing stiffness and energy dissipation. The theoretical strength predictions align with experimental findings. Ghaedi et al. [29] present a study on the BD, a new metallic damper designed to enhance the cyclic performance of semi-rigid frames. The damper consists of solid bars between the top and bottom plates, dissipating external energy through plastic deformation. Evaluations included pushover analysis, quasi-static cyclic tests, and three-dimensional finite element models, which validated that the bar damper significantly improved frame strength, effective stiffness, damping ratio, and energy dissipation capacity. Rahimi et al. [30] explore the impact of lateral bearing systems on rehabilitating reinforced concrete frames, focusing on Non-uniform Slit Dampers and Bar dampers. They constructed three one-third-scale experimental samples and developed sixteen numerical models to assess the dampers' effects on stiffness, strength, ductility, and energy dissipation. Findings demonstrate significant improvements in seismic performance with these dampers, and fewer dampers can still enhance seismic parameters without reducing cyclic capacity.

One of the parameters affecting the behavior of yielding dampers is axial force. Axial force is applied to the damper depending on its location in the structure. Several past studies have addressed this topic. Mortezagholi et al. [31] examined the impact of axial forces on Added damping and stiffness (ADAS) dampers, noting their role in increasing strain and affecting ductility. They introduced Modified ADAS (MADAS) to prevent these effects. Experimental and numerical evaluations showed MADAS maintained consistent force levels and better cyclic durability, unlike ADAS, which caused brace buckling under increased forces. Cheraghi et al. [32] investigated ADAS dampers to derive equations for calculating seismic parameters. They employed a model to analyze various variables, proposing equations for stiffness, energy dissipation, and strength. The study identified variables with significant and minimal impact on results, examining the influence of axial force, critical load, and geometric modifications on damper performance, including stiffness, strength, and ductility. Khoshkalam et al. [33] examined various yielding dampers to enhance seismic performance, focusing on ADAS dampers, which struggle with tensile axial forces during large deformations. These forces lead to strain localization and damage. The study introduced a modified ADAS damper, redirecting axial forces to bracings. Using

Abaqus, an equation for maximum shear stress was proposed, showing MADAS dampers with superior energy dissipation and reduced plastic strain.

In previous studies, the effect of axial force on the cyclic behavior of BD has not been investigated. The location of the damper, as well as the BD, has been proposed in many past studies, as shown in Fig. 1 [34–37]. In this arrangement, dead and live loads cause beam deflection and apply forces to the dampers. In Fig. 1, Fx and Fz represent the lateral and axial forces on the dampers, respectively.

If drift occurs in the frame, additional moments are generated in the damper due to this axial force, leading to changes in their overall behavior. If the frame is semi-rigid, the weaker frame connection results in greater forces being applied to these dampers. Understanding which parameter of the damper is most affected by the axial force significantly aids structural designers in making more informed design decisions.

This study focused on the influence of axial force on the cyclic performance of the BD. The analyses conducted in this study were cyclic. To validate the numerical results, three experimental BD specimens with different heights were utilized. The buckling load of the damper was calculated by solving the differential equation governing the buckling behavior of the damper, and the effects of 2% and 4% axial force on its cyclic performance were evaluated.

2 Validation of the numerical model

The studies conducted in this research were carried out using the ABAQUS finite element software [38]. An experimental sample was utilized to ensure the accuracy of the Finite Element (FE) model.

Fig. 2(a) shows the experimental sample tested by Ghaedi et al. [28]. Three experimental samples from this study were used to validate the numerical model. Each of the experimental models included 24 BDs. These 24 BDs had a diameter of 10mm and heights of 70 mm, 100 mm, and 130 mm. The lower plate of these models was fixed, and loading was applied cyclically to the upper plate. The loading history is shown in Fig. 2(b). The material properties of the dampers were reported with a yield stress of 341.2 MPa and an ultimate stress of 532.3 MPa. Failure was reported at the connection of the BD in these models at the end of the loading.

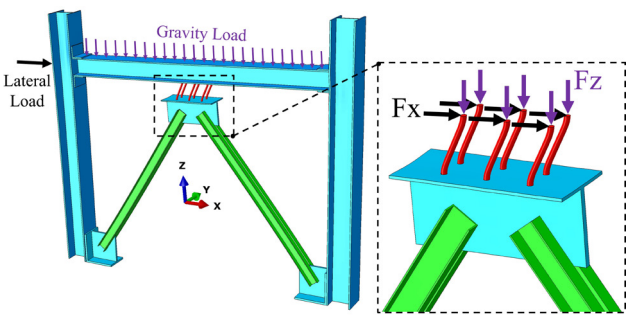

Fig. 1 The application of axial force to the BD in the frame subjected to lateral load

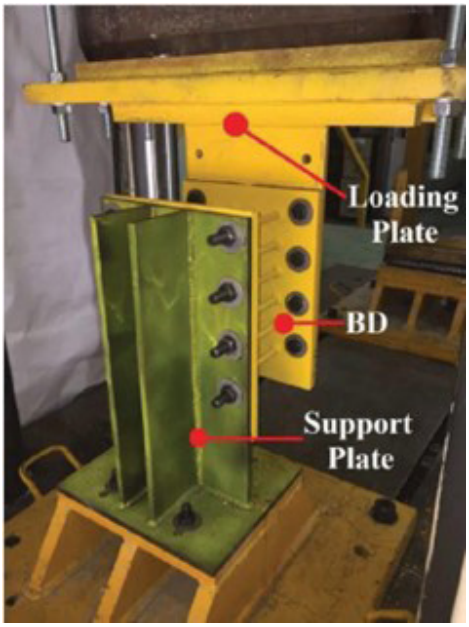

(a)

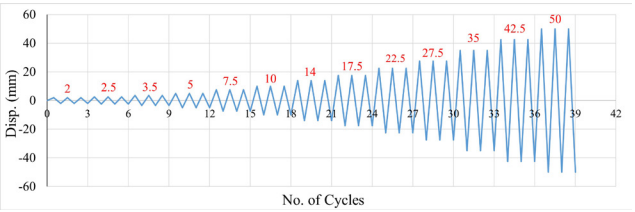

(b)

Fig. 2 (a) Experimental specimen [28] (b) Loading history of the models

Eight-node solid elements were employed to simulate the numerical model. These elements, which have 24 degrees of freedom, were used in the Incompatible Mode (C3D8I). Incompatible Mode in Abaqus enhances element deformation accuracy by introducing extra degrees of freedom, reducing shear locking. The analysis utilized the Static General solver, incorporating large deformations and strain hardening. The numerical analysis in ABAQUS was performed with an increment length of 0.05 in the static general step, chosen to balance accuracy and computational time. In the experimental models, no connection failure occurred until the end of loading. Therefore, the "Tie" constraint was used for the connections in the numerical

model. In ABAQUS, "Tie" constraints are used to bond two separate regions together, ensuring they share the same deformations and stresses [38]. The analysis of the models was performed using the displacement-control method. The Young's modulus (E) was set to 200 GPa. To accurately model the cyclic response, a kinematic hardening model was employed with a hardening modulus of 800 MPa.

Six numerical analyses were conducted to determine appropriate mesh dimensions and evaluate the effect of mesh size on the hysteresis loop area (E_{loop}) and maximum strength. In the convergence study, a mesh size was adopted that represents a practical balance between accuracy and computational cost, providing reliable results while avoiding unnecessary computational overhead. Based on Table 1, the mesh size was set to 4 mm. Fig. 3 shows the meshed model and its boundary conditions, which were defined based on the experimental model.

The stress results for one of the models are shown in Fig. 4(a), corresponding to the maximum displacement. It is observed that the maximum stresses occur in areas near the connection. Fig. 4(b) illustrates the failure mode of the experimental specimen, revealing that the failures at the final moment happened in the connections, which were the locations of maximum stress in the numerical model. The comparison of numerical and experimental hysteresis results is presented in Fig. 5. These results pertain to three experimental specimens with different heights. It is observed that the numerical model has performed satisfactorily in computing the results.

Table 1 Mesh sensitivity analysis results

No. of model	Mesh size of BD (mm)	Error (%) relative to model 4	
		Strength	E_{loop}
1	8	5.28	4.91
2	6	4.33	1.11
3	4	0.93	0.54
4	2	0	0
5	1	0.3	0.08
6	0.5	0.33	0.09

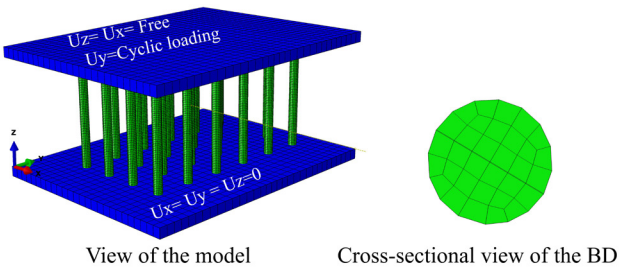

Fig. 3 The meshed model and its boundary conditions

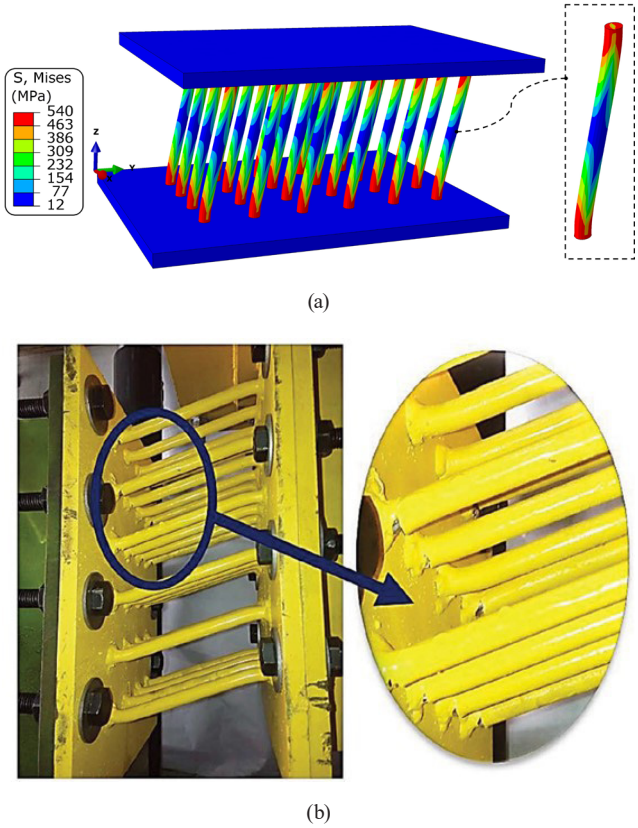

Fig. 4 (a) Stress results of the model at maximum displacement, (b) failure mode of the experimental specimen [28]

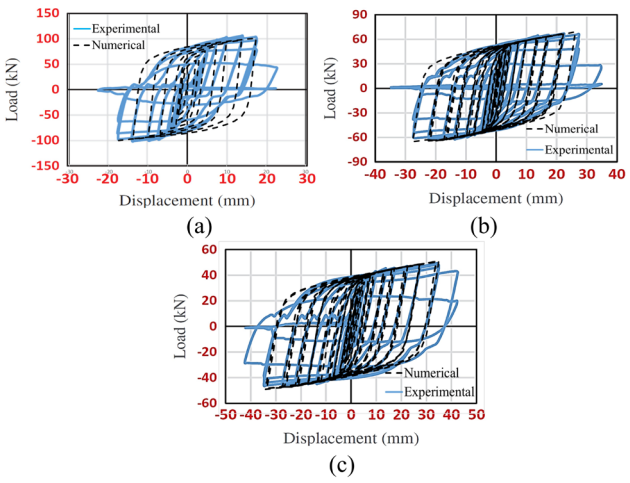

Fig. 5 Comparison of numerical and experimental results for models with heights: (a) 70 mm, (b) 100 mm, (c) 130 mm

3 Buckling load of the BD

When the damper is positioned, as shown in Fig. 3, the slope at both ends becomes zero after lateral deformation. Therefore, the mathematical model of the damper can be

represented as shown in Fig. 6. The governing equation for the buckling of this damper is given in Eq. (1).

$$y''''(x)+\frac{P}{EI}y''(x)=0 \quad I=\frac{\pi D^4}{64} \tag{1}$$

Thus, Eq. (1) can be solved with three boundary conditions as specified in Eq. (2). This formulation is derived assuming lateral force $F = 0$, which makes the boundary condition of zero shear valid at the free end.

$$y_{(0)}=0, \quad y'_{(0)}=y'_{(H)}=0, \quad y'''_{(H)}=0 \tag{2}$$

Two of the boundary conditions specify zero slope at both ends, one boundary condition specifies zero displacement at the fixed end, and one boundary condition specifies zero shear force at the free end. By solving Eq. (1), the buckling load is obtained as Eq. (3). In Eqs. (1)-(3), E and I represent Young's modulus and moment of inertia of the BD. Height and diameter are denoted as H and D.

Following Ghaedi et al. [28], the elastic stiffness of a single bar damper is given by Eq. (4) with $N = 1$. Under rigid end plates and uniform load distribution, N bars act as parallel springs, so the total elastic stiffness equals the sum of the individual stiffnesses, i.e., Eq. (4).

$$Pcr=\frac{\pi^2 EI}{H^2} \tag{3}$$

$$K_e=N\frac{12EI}{H^3} \tag{4}$$

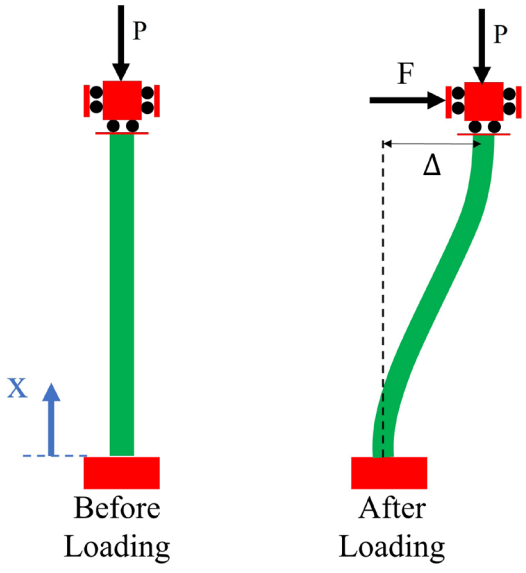

Fig. 6 Mathematical model of BD under axial force

4 Impact of axial force on the cyclic behavior of dampers

This section examines the effect of axial force on the hysteresis behavior of the BD. If the damper is not subjected to axial force, its schematic hysteresis curve during one loading cycle is shown in Fig. 7. In this figure, the method for calculating the damper's effective stiffness (K_{eff}) is also illustrated. Additionally, based on Eq. (5), the EDR can be determined.

$$\xi=\frac{E_{loop}}{2\pi K_{eff}\delta_{\max}^2} \tag{5}$$

However, when axial force is applied, its behavior changes and becomes dependent on the damper's position relative to its initial state. For a more detailed examination of this condition, the hysteresis curve of the damper under axial force is presented in Fig. 8. This figure provides a schematic view of the hysteretic path under combined axial and lateral loading. It is presented only as a conceptual

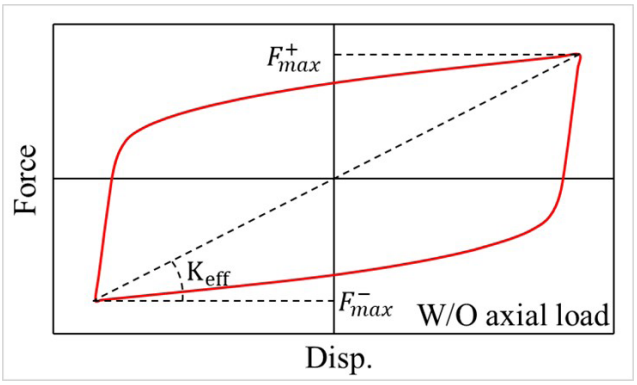

Fig. 7 Hysteresis curve of the damper without axial force

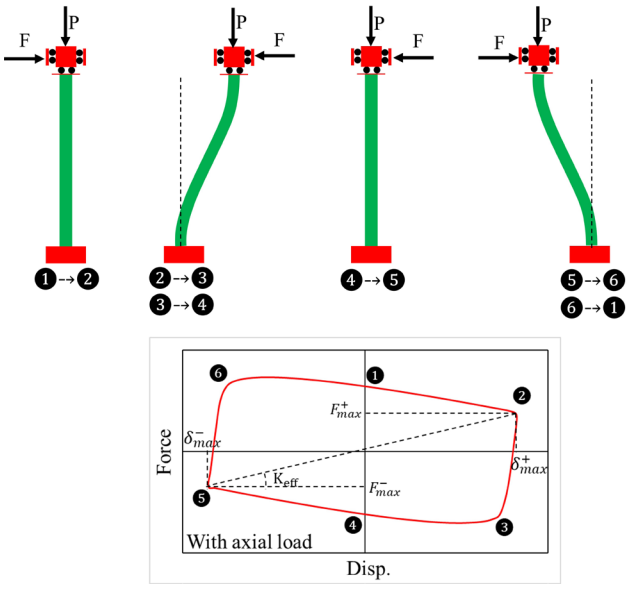

Fig. 8 Hysteresis curve of the damper with axial force

illustration to highlight the difference between active and passive plastic states, rather than as a representative numerical result. The actual cyclic responses of the damper, including the observed reduction in post-yield hardening due to axial force, are reflected in the numerical analyses shown in Figs. 9 and 10. Fig. 10 examines the damper's response under both axial and lateral forces during one loading cycle in six different positions. If the damper is in position 1 to 2 and the lateral force is applied in the positive direction, its effect combines with the effect of the axial force. In this case, the impact of the axial force is significant. In positions 2 to 3 and 3 to 4, the effect of axial force counteracts the lateral force, thus requiring a greater lateral force to return the damper to its initial position. The behavior in positions 4 to 5 is similar to that from 1 to 2. Finally, for the transition from 5 to 6 and 6 to 1, a large lateral force is again needed, as the axial force acts as a resisting force. Therefore, the critical positions of the damper under axial force are at positions 2 and 5. A notable point in this curve is that at position 6, the axial force has a greater effect on the damper due to the large displacement. At this position, a significant lateral force is required to maintain equilibrium.

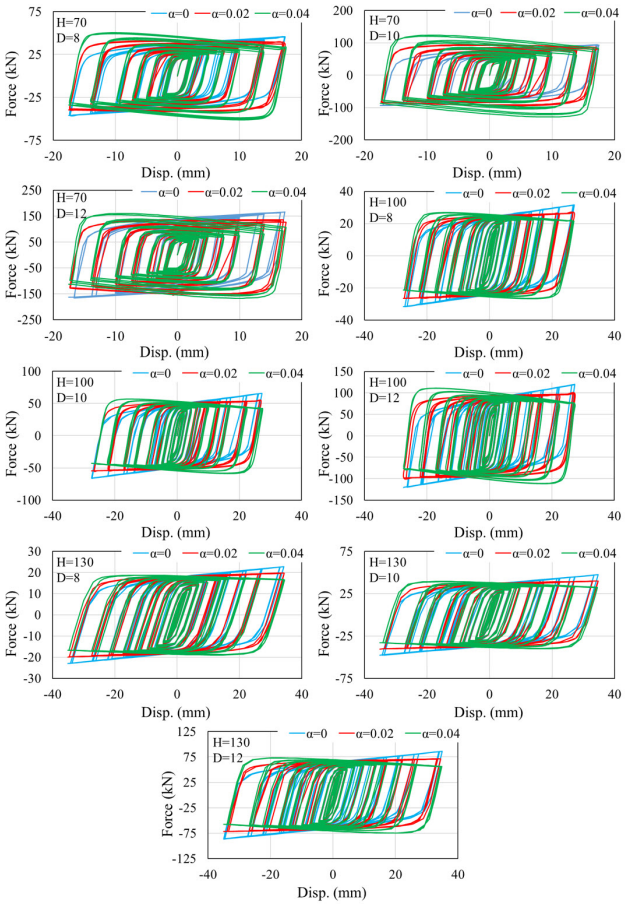

Fig. 9 Hysteresis curve results

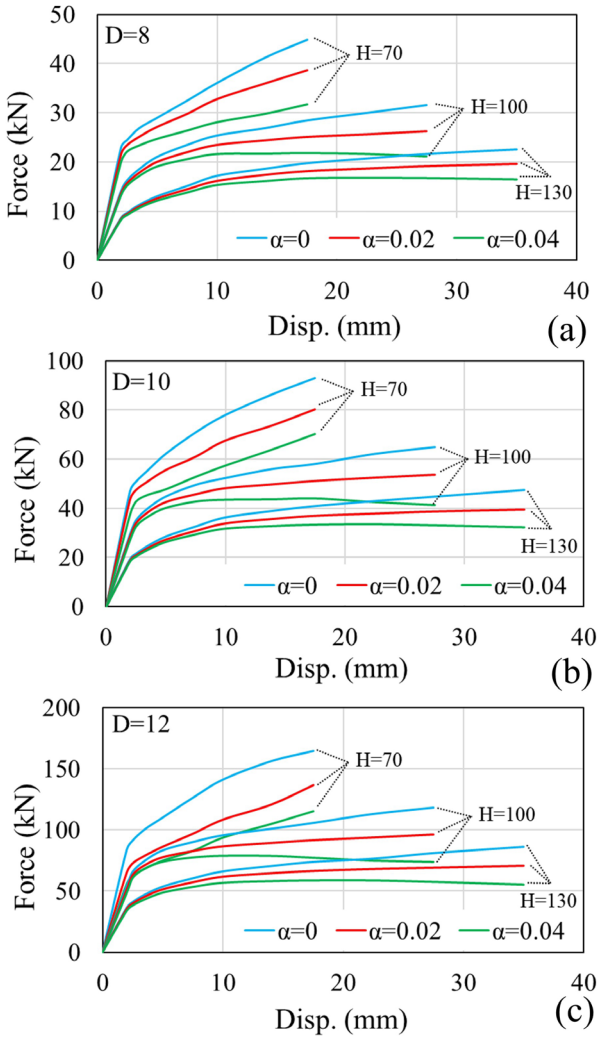

Fig. 10 Skeleton curves of models: (a) D = 8 mm, (b) D = 10 mm, and (c) D = 12 mm

As the displacement approaches zero, the influence of the axial force diminishes, and the lateral force also decreases.

This hysteretic behavior under combined loading can be explained more rigorously using the concepts of active and passive plastic states. During the 'active' phase (e.g., paths 1-to-2 and 4-to-5), the *P*-delta moment generated by the axial force acts in the same direction as the lateral force, thereby amplifying the deformation. Conversely, during the 'passive' phase of unloading and reloading (e.g., paths 2-to-4 and 5-to-1), the *P*-delta moment opposes the restoring force, thus requiring a larger lateral force to return the damper towards its initial position

5 Parametric study

In this section, numerical studies were conducted to investigate the effect of axial force on the cyclic performance of the BD. The model under study in this section is defined

as shown in Fig. 11. The only difference between this model and the validation model is the addition of axial force. The analysis of this model was carried out in two steps. In the first step, only the axial force was applied, and the lateral cyclic force was introduced in the second step. Fig. 11 also illustrates these boundary conditions. All models studied in this section are defined in Table 2. The naming of each model is based on the dimensions and axial force of the damper. In this table, α represents the ratio of the applied axial load to the buckling load of the damper.

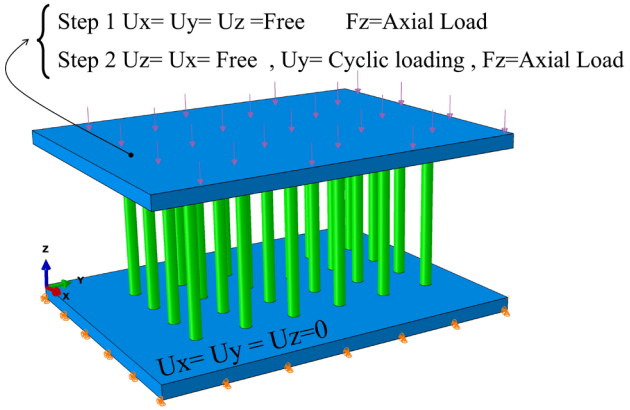

Fig. 11 Boundary conditions of the parametric models

In this table, the results of elastic stiffness, which represents the initial slope of the force-displacement curve, obtained from numerical analyses are presented. Additionally, the results from Eq. (4) are also provided. In Eq. (4), the effect of axial force is not considered, and this equation is only applicable to the model without axial force. Numerical analyses showed that axial force reduces the initial stiffness of the damper. Therefore, Eq. (6) is proposed based on curve-fitting methods to incorporate the effect of axial force on elastic stiffness. The numerical analyses (Table 2) confirmed that this relation provides good

Table 2 Specifications of parametric models and elastic stiffness results

B-H-D-α	Dimensions of BD (mm)			Axial load (kN)	K_e (kN/mm)			Normalized K_e
	H	D	α		Eq. (4)	Numerical	Eq. (6)	
B-70-8-0			0	0	33.76	32.66	33.76	1
B-70-8-0.02		8	0.02	38.88	-	31.64	32.69	0.97
B-70-8-0.04			0.04	77.76	-	30.64	31.69	0.94
B-70-10-0			0	0	82.43	79.97	82.43	1
B-70-10-0.02	70	10	0.02	94.92	-	77.49	79.82	0.97
B-70-10-0.04			0.04	189.83	-	75.07	77.37	0.92
B-70-12-0			0	0	170.93	165.34	170.93	1
B-70-12-0.02		12	0.02	196.82	-	160.26	165.51	0.97
B-70-12-0.04			0.04	393.64	-	155.29	160.43	0.94
B-100-8-0			0	0	11.58	11.43	11.58	1
B-100-8-0.02		8	0.02	19.05	-	11.07	11.21	0.97
B-100-8-0.04			0.04	38.1	-	10.72	10.87	0.94
B-100-10-0			0	0	28.27	27.96	28.27	1
B-100-10-0.02	100	10	0.02	46.51	-	27.09	27.38	0.97
B-100-10-0.04			0.04	93.02	-	26.24	26.54	0.94
B-100-12-0			0	0	58.63	57.83	58.63	1
B-100-12-0.02		12	0.02	96.44	-	56.04	56.77	0.97
B-100-12-0.04			0.04	192.88	-	54.3	55.03	0.94
B-130-8-0			0	0	5.27	5.18	5.27	1
B-130-8-0.02		8	0.02	11.27	-	5.02	5.1	0.97
B-130-8-0.04			0.04	22.54	-	4.86	4.95	0.94
B-130-10-0			0	0	12.87	12.69	12.87	1
B-130-10-0.02	130	10	0.02	27.52	-	12.3	12.46	0.97
B-130-10-0.04			0.04	55.04	-	11.91	12.08	0.94
B-130-12-0			0	0	26.69	26.35	26.69	1
B-130-12-0.02		12	0.02	57.07	-	25.53	25.84	0.97
B-130-12-0.04			0.04	114.13	-	24.73	25.05	0.94

agreement with the results for all examined damper heights H = 70, 100, and 130 mm. While more complex formulations could be developed, the proposed function offers a simple and sufficiently accurate estimate within its calibration range. It should be emphasized, however, that the validity of Eq. (6) is limited to small axial-force ratios ($0 \le \alpha \le 0.04$) and it does not provide acceptable results for other ranges.

$$K_{e_p} = \frac{1}{1+1.637\alpha}\left(N\frac{12EI}{H^3}\right) \tag{6}$$

After analyzing the models defined in Table 2, their hysteresis curves were obtained as shown in Fig. 9. In this figure, the models with constant diameter and height are presented separately. The cyclic responses under axial force are quantified by the numerical hysteresis loops in Fig. 9 and the skeleton curves in Fig. 10, while Fig. 8 serves only as a schematic illustration of the active and passive path features. Subsequently, the essential seismic parameters were extracted from these diagrams and analyzed.

The skeleton curve results of the models are presented in Fig. 10. Each of these figures illustrates the results of the models with a constant diameter. The presence of axial force reduces the post-yield hardening stiffness of the damper due to the *P*-delta effect. As observed in the numerical results (Fig. 9), this effect is moderate for small axial forces (e.g., α = 0.02), resulting in a lower hardening slope. However, it can lead to significant softening (a negative tangent stiffness) at larger axial force ratios (e.g., α = 0.04) and large displacements, where the *P*-delta effect overcomes the material's natural strain hardening.

One of the important parameters of yielding dampers is their effective stiffness, which can be calculated based on Fig. 8. The effective stiffness of the damper depends on its displacement. As the displacement approaches zero, the effective stiffness tends to the damper's initial stiffness. As observed, an increase in displacement leads to a significant reduction in the effective stiffness of the models. This rate of stiffness degradation is most pronounced for the models with a lower height (H = 70 mm).

Furthermore, across all models, an increase in axial force consistently causes a further reduction in effective stiffness. It should be noted that, unlike the theoretical elastic stiffness, the variation in effective stiffness between the different geometries does not follow a simple inverse cubic relationship with the damper height (H3).

The focus of this section is to examine the EDR of the models, which can be calculated using Eq. (5). In many previous studies, this parameter has been calculated for metallic dampers [39–42]. Fig. 12 illustrates the variations in EDR with respect to displacement.

In this figure, the EDR results for models with a constant diameter are shown in three pairs of plots. It can be observed that in all models, an increase in axial force leads to an increase in EDR. As the displacement of the dampers increases, the influence of axial force on these results becomes more pronounced. According to Eq. (5), EDR depends on the energy dissipation and effective stiffness of the damper. Since axial force had a negligible effect on energy absorption, EDR becomes dependent on effective stiffness. Fig. 13 shows that increasing axial force reduces effective stiffness. Therefore, the reduction in effective stiffness results in an increase in EDR. Additionally, these results show that the height and diameter of the damper have had a negligible impact on it.

Table 3 presents the normalized result of maximum strength, effective stiffness, energy dissipation, and EDR. In this table, the normalized values represent the ratio of each parameter in the presence of axial force to that of the corresponding model without axial force. For example, a value of 0.87 means that the result of the model with axial force is 87% of the value obtained for the same model without axial force.

Table 3 presents a quantitative summary of the key seismic parameters, normalized by the results of the corresponding model without axial force α = 0. The first column now represents the damper slenderness ratio (H/D) for the three main groups of models with heights of 70, 100, and 130 mm. The data shows a consistent trend of degradation in strength and stiffness with increasing axial force.

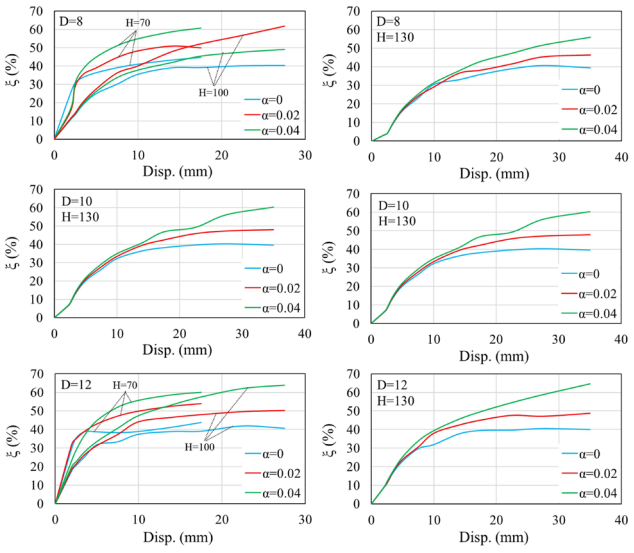

Fig. 12 Results of EDR in the models at various damper displacements (Units:mm)

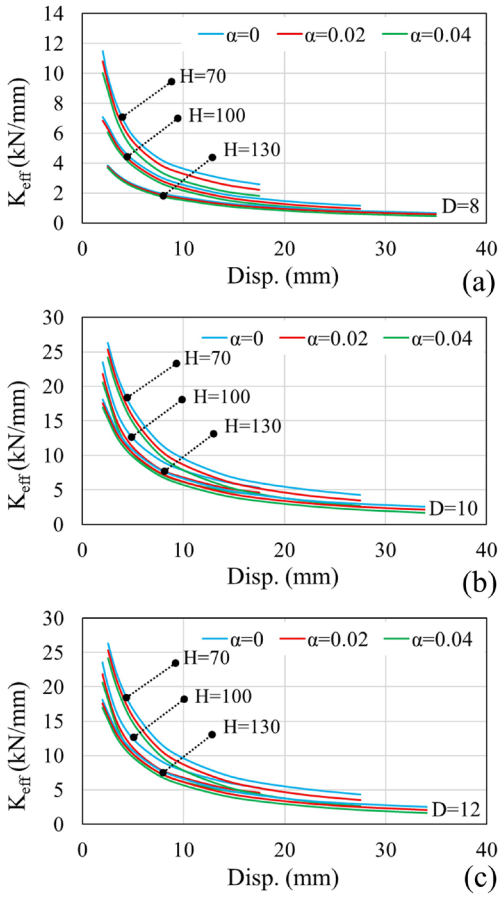

Fig. 13 Results of the effective stiffness of the models relative to damper displacement (units:mm): (a) D = 8 mm, (b) D = 10 mm, and (c) D = 12 mm

For an axial force ratio of $\alpha = 0.04$, the maximum strength is reduced by an average of 30%, and the effective stiffness by 11%. In stark contrast, the total energy dissipation was found to be largely unaffected, with variations of less than 5% across all slenderness ratios.

Conversely, the EDR generally increases with axial force, with an average rise of 18% for $\alpha = 0.04$. This trend is directly linked to the consistent energy dissipation and reduced effective stiffness. More importantly, the data reveals a clear relationship between the slenderness ratio and the severity of these effects. For instance, in the group of dampers with $H = 70$ mm (lower slenderness ratios), the impact is most pronounced, with a strength reduction of up to 30% and a stiffness reduction of up to 33%. In contrast, for dampers with $H = 130$ mm (higher slenderness ratios), the degradation is less severe, and the EDR shows minimal changes. This indicates that dampers with a lower slenderness ratio (H/D) are more sensitive to the detrimental effects of axial force. This finding underscores a critical aspect of the damper's behavior: while the axial force has a minimal impact on the cumulative energy dissipation, it fundamentally alters the overall seismic performance by causing a significant degradation in strength and stiffness.

Analysis of the average results indicates that axial force has its greatest influence on maximum strength, causing a notable reduction (averaging 30%), and on the equivalent damping ratio, leading to a significant increase (averaging 18%). Since stiffness significantly influences the dynamic behavior of structures equipped with yielding dampers, this effect must be considered in the design process.

6 Evaluation of stress in the models

In this section, the stress distribution of the models is examined. Since the displacement of the BDs in the model is identical, their behavior resembles a system with parallel springs. Consequently, they experience the same stress. Therefore, the stress results are presented for only one BD in Fig. 14. The von Mises stress distribution for a representative bar from selected models is presented in Fig. 14. The figure illustrates the stress state at the point of maximum displacement for three dampers with different heights ($H = 70$, 100, and 130 mm) under varying axial force ratios ($\alpha = 0$,0.02, and 0.04). Regions where the stress exceeds the material's yield strength (347 MPa) are depicted in gray.

The results clearly demonstrate that for all geometries, increasing the axial force leads to a significant increase in the peak von Mises stresses. In all cases, the maximum stresses are concentrated at the connections to the top and bottom plates, which is the location of maximum bending moment. Due to the symmetric boundary conditions, an inflection point with zero internal moment forms at the damper's mid-height, which is consistently the region of lowest stress, irrespective of the presence of axial force.

$$\sigma_v = \sqrt{\frac{1}{2}\left[\begin{array}{l}\left(\sigma_{11}-\sigma_{22}\right)^2+\left(\sigma_{22}-\sigma_{33}\right)^2\\ +\left(\sigma_{33}-\sigma_{11}\right)^2\end{array}\right] +3\left(\sigma_{12}^2+\sigma_{23}^2+\sigma_{13}^2\right)} \tag{7}$$

The results of the models up to this point demonstrated that axial force alters the cyclic behavior of the damper. Changes in parameters such as stiffness also affect the dynamic behavior of the damper, which must be considered in structures equipped with this type of damper. These dampers experience maximum moments at the connection points. Therefore, the connection must be designed to prevent failure throughout the loading process. The number of dampers in this study was 24. These dampers function as parallel springs in the model. Thus, the findings of this study can be extended to different dimensions. As observed, the

Table 3 Normalized results of the models compared to the model without axial force

H	$\frac{H}{D}-\alpha$	Normalized strength	Normalized effective stiffness	Normalized energy dissipation	Normalized EDR
	8.75-0	1	1	1	1
	8.75-0.02	0.86	0.94	1.01	1.13
	8.75-0.04	0.71	0.87	1.02	1.36
	7-0	1	1	1	1
70	7-0.02	0.86	0.93	1.01	1.16
	7-0.04	0.75	0.88	1.02	1.25
	5.83-0	1	1	1	1
	5.83-0.02	0.83	0.78	0.97	1.23
	5.83-0.04	0.7	0.67	0.95	1.37
	12.5-0	1	1	1	1
	12.5-0.02	0.83	0.97	0.99	1.13
	12.5-0.04	0.69	0.94	0.98	1.26
	10-0	1	1	1	1
100	10-0.02	0.83	0.96	0.99	1.14
	10-0.04	0.68	0.92	0.98	1.34
	8.33-0	1	1	1	1
	8.33-0.02	0.82	0.96	0.98	0.92
	8.33-0.04	0.66	0.9	0.97	1.06
	16.25-0	1	1	1	1
	16.25-0.02	0.87	0.98	0.98	0.99
	16.25-0.04	0.74	0.95	0.98	1
	13-0	1	1	1	1
130	13-0.02	0.84	0.98	0.98	1.01
	13-0.04	0.71	0.95	0.97	1
	10.83-0	1	1	1	1
	10.83-0.02	0.82	0.97	0.98	1.02
	10.83-0.04	0.69	0.94	0.96	1.03

number of dampers was also included in the stiffness equation. The impact of axial force on dampers with varying dimensions was nearly the same. It is worth noting that the axial force for each damper was applied based on its critical load. If the axial force remains constant, increasing the diameter and reducing the height of the BD can mitigate the negative effects of the axial force.

It should be noted that the assumption of uniform axial force distribution among the dampers is considered valid in this study. This assumption is justified by the significant thickness and resulting high rigidity of the loading plates, combined with the load being applied uniformly over the plate's surface, which prevented any observable plate deformation.

7 Conclusions

This study was conducted to investigate the effect of axial force on the cyclic behavior of BD through a parametric analysis. Initially, three experimental BD samples with different heights were used to validate the numerical results. The buckling load of the damper was then calculated by solving the differential equation governing its buckling behavior. To evaluate the effect of this axial force on the damper, 27 nonlinear static analyses were performed. The model variables included the damper dimensions and its axial force. Axial force was applied at 2% and 4% of the buckling load. Subsequently, the seismic results of the damper, including elastic stiffness, strength, effective stiffness, energy absorption, and EDR, were calculated. An approximate equation was proposed to estimate the elastic stiffness of the damper under axial force, which showed good agreement with the numerical results. After reviewing the results, the summary is presented as follows.

- The results showed that the axial force reduces the elastic stiffness of the damper. Based on the direct average of the numerical results, this reduction was

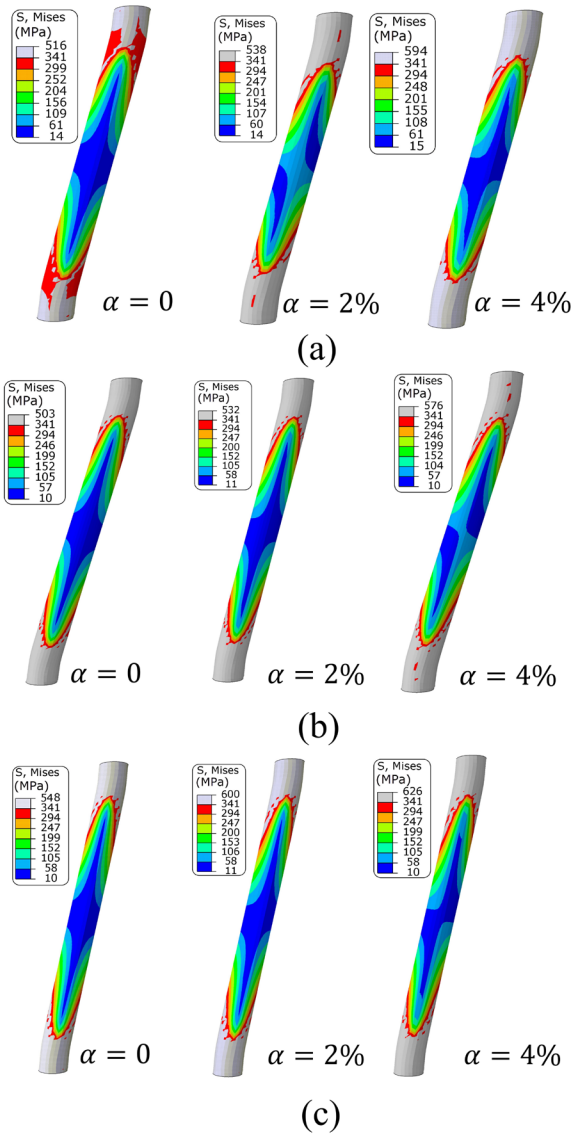

Fig. 14 Stress distribution for the models: (a) $H = 70$, $D = 8$, (b) $H = 100$, $D = 10$, and (c) $H = 130$, $D = 12$

3% and 6% for axial force ratios of $\alpha = 0.02$ and $\alpha = 0.04$, respectively. The proposed approximate equation showed reasonable agreement with these observed numerical trends.

- Axial force reduced the effective stiffness of the damper, but its impact on energy absorption was minimal. A 2% and 4% increase in axial force led to a 5.8% and 11% decrease in effective stiffness, respectively. However, the effect on energy absorption was calculated to be less than 0.5%.
- A key finding is the significant increase in the EDR under axial force, with an average rise of up to 18%. This result is a direct consequence of the interplay between the damper's stiffness and its energy dissipation capacity. The analysis revealed that while the cumulative energy dissipated per cycle remained remarkably constant, the effective stiffness was significantly degraded due to the *P*-delta effect. Since the EDR is proportional to the ratio of dissipated energy to effective stiffness, the pronounced reduction in stiffness was the primary driver for the observed enhancement in damping, an effect that was most pronounced at larger displacements.
- The application of axial force caused a significant reduction in the damper's strength, an effect that was more pronounced at larger displacements due to the *P*-delta mechanism. Quantitatively, applying axial forces of 2% and 4% of the damper's critical load resulted in average reductions in maximum strength of 16% and 30%, respectively.
- While the numerical model in this study comprised 24 individual bar dampers to replicate the experimental setup, the analysis confirmed they exhibit parallel mechanical behavior. Therefore, a valuable direction for future research would be to investigate the efficacy of a simplified, single-bar equivalent model. Such an approach promises to significantly reduce computational costs, streamlining the analysis and design process for structures incorporating these dampers.
- Future research could extend the present analysis to investigate dampers with low aspect ratios (i.e., larger diameters relative to height), in order to quantify the contribution of shear deformations to the overall hysteretic response and energy dissipation capacity.

Nomenclature

D	The diameter of the BD
H	Height of the BD
α	The ratio of the axial force of the BD to its critical load
N	The number of BD in a model
Pcr	The buckling load of BD
E	Young's modulus of the BD
I	Moment of inertia of the BD
K_e	The elastic stiffness of the damper without axial force
K_{e_p}	The elastic stiffness of the BD with axial force
K_{eff}	The effective stiffness of the BD
ξ	The equivalent damping ratio of the proposed damper

References

[1] Cheraghi, K., TahamouliRoudsari, M., Kiasat, S., Esfandiari, J. "Numerical Investigation of Cyclic Behavior of Angled U-shaped Yielding Damper on Steel Frames", Periodica Polytechnica Civil Engineering, 68(2), pp. 426–434, 2024. https://doi.org/10.3311/PPci.23213

[2] Nazeran, R., Hemmati, A., Kazemi, H. "Numerical and experimental behavior of moment concrete frame retrofitted with TADAS metal yielding damper under lateral loading", Structural Engineering and Mechanics, 89(5), pp. 507–524, 2024. https://doi.org/10.12989/sem.2024.89.5.507

[3] Bigdeli, A., Rahman, M.M., Kim, D. "Vibration control of low-rise buildings considering nonlinear behavior of concrete using tuned mass damper", Structural Engineering and Mechanics, 88(3), pp. 209–220, 2023. https://doi.org/10.12989/sem.2023.88.3.209

[4] Xiang, N., Jian, N., Nonaka, T. "A novel longitudinal seismic self-centering system for RC continuous bridges using SMA rebars and friction dampers", Structural Engineering and Mechanics, 82(4), pp. 435–444, 2022. https://doi.org/10.12989/sem.2022.82.4.435

[5] Saeidzadeh, M., Chenaghlou, M. R., Akbari Hamed, A. "Experimental and numerical study on the performance of a novel self-centering beam-column connection equipped with friction dampers", Journal of Building Engineering, 52, 104338, 2022. https://doi.org/10.1016/j.jobe.2022.104338

[6] Akbari Hamed, A., Mortazavi, S. F., Saeidzadeh, M. "Evaluation of the seismic performance of structures equipped with novel multi-level TADAS dampers", Asian Journal of Civil Engineering, 24(4), pp. 969–988, 2023. https://doi.org/10.1007/s42107-022-00546-5

[7] Vafadar, F., Broujerdian, V., Ghamari, A. "Improving the seismic behavior of diagonal braces by developing a new combined slit damper and shape memory alloys", Structural Engineering and Mechanics, 82(1), pp. 107–120, 2022. https://doi.org/10.12989/sem.2022.82.1.107

[8] Aghani, H., Cheraghi, K., Bakhshipour, M. "Numerical Investigation of the Effect of Aluminum Yielding Damper for the Retrofitting of Semi-rigid Steel Frames", Periodica Polytechnica Civil Engineering, 68(2), pp. 349–357, 2024. https://doi.org/10.3311/PPci.23119

[9] Gharra, K., Khanlari, K., Asgari Marnani, J. "A Simplified Matrix Analysis Approach to Multi-story Buildings Involving a Friction Damper", Periodica Polytechnica Civil Engineering, 66(1), pp. 75–85, 2022. https://doi.org/10.3311/PPci.18558

[10] Hashemi, M. R., Vahdani, R., Gerami, M., Kheyroddin, A. "A New Approach to the Optimal Placement of the Viscous Damper Based on the Static Force Distribution Pattern", Periodica Polytechnica Civil Engineering, 66(3), pp. 866–875, 2022. https://doi.org/10.3311/PPci.17238

[11] Cheraghi, K., Tahamouli Roudsari, M., Kiasat, S., Cheraghi, K. "Numerical and analytical investigation of cyclic behavior of D-Shape yielding damper", Structural Engineering and Mechanics, 89(4), 411, 2024. https://doi.org/10.12989/sem.2024.89.4.411

[12] Shahri, S. F., Mousavi, S. R. "Seismic behavior of beam-to-column connections with elliptic slit dampers", Steel and Composite Structures, 26(3), pp. 289–301, 2018. https://doi.org/10.12989/scs.2018.26.3.289

[13] Lotfi Mahyari, S., Tajmir Riahi, H., Hashemi, M. "Investigating the analytical and experimental performance of a pure torsional yielding damper", Journal of Constructional Steel Research, 161, pp. 385–399, 2019. https://doi.org/10.1016/j.jcsr.2019.07.010

[14] Gorji Azandariani, M., Gorji Azandariani, A., Abdolmaleki, H. "Cyclic behavior of an energy dissipation system with steel dual-ring dampers (SDRDs)", Journal of Constructional Steel Research, 172, 106145, 2020. https://doi.org/10.1016/j.jcsr.2020.106145

[15] Ghamari, A., Kim, Y.-J., Bae, J. "Utilizing an I-shaped shear link as a damper to improve the behaviour of a concentrically braced frame", Journal of Constructional Steel Research, 186, 106915, 2021. https://doi.org/10.1016/j.jcsr.2021.106915

[16] Zhou, X., Tan, Y., Ke, K., Yam, M.C.H., Zhang, H., Xu, J. "An experimental and numerical study of brace-type long double C-section steel slit dampers", Journal of Building Engineering, 64, 105555, 2023. https://doi.org/10.1016/j.jobe.2022.105555

[17] Yang, J., Liang, S., Zhu, X., Dang, L., Shen, T., Zhou, S. "Experimental and theoretical research on a shear-bending-metallic-damper with a double-phased yield mechanism", Journal of Constructional Steel Research, 203, 107839, 2023. https://doi.org/10.1016/j.jcsr.2023.107839

[18] Qiu, C.-X., Huang, T.-Y., Wang, Y.-Z., Qian, H.-J. "Theoretical and experimental study on seismic performance of T-section metallic damper", Journal of Constructional Steel Research, 211, 108161, 2023. https://doi.org/10.1016/j.jcsr.2023.108161

[19] Cheraghi, K., TahamouliRoudsari, M. "Analytical and numerical investigation of the cyclic behavior of angled U-shape damper", Steel and Composite Structures, 51(3), pp. 325–335, 2024. https://doi.org/10.12989/scs.2024.51.3.325

[20] Deng, K., Liang, H., Yi, Y., Zhao, C., Dai, S., Wu, D. "Sliding U-shaped steel damper for multi-directional displacement", International Journal of Non-Linear Mechanics, 156, 104483, 2023. https://doi.org/10.1016/j.ijnonlinmec.2023.104483

[21] Cheraghi, K., TahamouliRoudsari, M., Kiasat, S. "Numerical and analytical investigation of U-shape dampers and its effect on steel frames", Structures, 55, pp. 498–509, 2023. https://doi.org/10.1016/j.istruc.2023.06.037

[22] Mazzolani, F. M., Taiyari, F. "The Influence of the U-Shaped Damper Configuration on the Seismic Performance of Steel Building Frames", In: Mazzolani, F. M., Dubina, D., Stratan, A. (eds.) Proceedings of the 10th International Conference on Behaviour of Steel Structures in Seismic Areas, Springer Cham, 2022, pp. 650–658. ISBN 978-3-031-03811-2 https://doi.org/10.1007/978-3-031-03811-2_70

[23] Shirinkam, M. R., Razzaghi, J. "Experimental and analytical investigation on the behavior of metallic Box-Shaped Dampers (BSD)", Structures, 23, pp. 766–778, 2020. https://doi.org/10.1016/j.istruc.2019.12.018

[24] Guo, W., Li, S., Zhai, Z., Li, Z., Tan, S., Ding, F. "Seismic performance of a new S-shaped mild steel damper with varied yielding cross-sections", Journal of Building Engineering, 45, 103508, 2022. https://doi.org/10.1016/j.jobe.2021.103508

[25] Zhai, Z., Guo, W., Yu, Z., He, C., Zeng, Z. "Experimental and numerical study of S-shaped steel plate damper for seismic resilient application", Engineering Structures, 221, 111006, 2020. https://doi.org/10.1016/j.engstruct.2020.111006

[26] Guo, W., Wang, X., Yu, Y., Chen, X., Li, S., Fang, W., Zeng, C., Wang, Y., Bu, D. "Experimental study of a steel damper with X-shaped welded pipe halves", Journal of Constructional Steel Research, 170, 106087, 2020. https://doi.org/10.1016/j.jcsr.2020.106087

[27] Zhu, X., Dang, L., Liang, S., Zhang, M., Yang, J., Dai, X. "Development and Investigation of the Hysteretic Behavior of an X-Shaped Metal Damper with an Oblique Angle", Applied Sciences, 13(22), 12464, 2023. https://doi.org/10.3390/app132212464

[28] Ghaedi, K., Ibrahim, Z., Javanmardi, A., Rupakhety, R. "Experimental Study of a New Bar Damper Device for Vibration Control of Structures Subjected to Earthquake Loads", Journal of Earthquake Engineering, 25(2), pp. 300–318, 2021. https://doi.org/10.1080/13632469.2018.1515796

[29] Ghaedi, K., Javanmardi, A., Ibrahim, Z., Gordan, M., S. M. Rashid, R., Khatibi, H., Vaghei, R. "Experimental and numerical studies on the cyclic performance of structural frames equipped with bar dampers", Structures, 50, pp. 707–722, 2023. https://doi.org/10.1016/j.istruc.2023.02.070

[30] Rahimi, H., Esfandari, J., TahamouliRoudsari, M. "Experimental and Numerical Assessment of the Seismic Behavior of Non-uniform Slit Dampers and Bar Dampers in Moment Resisting Reinforced Concrete Frames", Periodica Polytechnica Civil Engineering, 68(1), pp. 314–324, 2024. https://doi.org/10.3311/PPci.22993

[31] Mortezagholi, M. H., Zahrai, S. M., Abbasi Shanbehbazari, R. "Cyclic Behavior of a Novel MADAS Damper with No Axial Force and Improved Seismic Performance (Experimental, Numerical, and Analytical Assessment)", Journal of Earthquake Engineering, 28(8), pp. 2249–2272, 2024. https://doi.org/10.1080/13632469.2023.2286378

[32] Cheraghi, K., Tahamouli Roudsari, M., Kiasat, S., Esfandiari, J. "Numerical and Analytical Study of the Cyclic Behavior of ADAS Damper and the Effect of Axial Force on its Behavior", Journal of Earthquake Engineering, pp. 1–18, 2024. https://doi.org/10.1080/13632469.2024.2345821

[33] Khoshkalam, M., Mortezagholi, M. H., Zahrai, S. M. "Proposed Modification for ADAS Damper to Eliminate Axial Force and Improve Seismic Performance", Journal of Earthquake Engineering, pp. 1–23, 2021. https://doi.org/10.1080/13632469.2020.1859419

[34] Bagheria, S., Hadidi, A., Alilou, A. "Heightwise Distribution of Stiffness Ratio for Optimum Seismic Design of Steel Frames with Metallic-Yielding Dampers", Procedia Engineering, 14, pp. 2891–2898, 2011. https://doi.org/10.1016/j.proeng.2011.07.364

[35] Ebadi Jamkhaneh, M., Ebrahimi, A. H., Shokri Amiri, M. "Experimental and Numerical Investigation of Steel Moment Resisting Frame with U-Shaped Metallic Yielding Damper", International Journal of Steel Structures, 19(3), pp. 806–818, 2019. https://doi.org/10.1007/s13296-018-0166-z

[36] Maleki, S., Mahjoubi, S. "Dual-pipe damper", Journal of Constructional Steel Research, 85, pp. 81–91, 2013. https://doi.org/10.1016/j.jcsr.2013.03.004

[37] Zheng, J., Li, A., Guo, T. "Analytical and experimental study on mild steel dampers with non-uniform vertical slits", Earthquake Engineering and Engineering Vibration, 14(1), pp. 111–123, 2015. https://doi.org/10.1007/s11803-015-0010-9

[38] Hibbitt, K., Sorensen, I. "ABAQUS/Standard User's Manual Volumes I–III and ABAQUS CAE Manual, Version 6.14", Hibbitt, Karlsson & Sorensen, 2014.

[39] Li, Q., Wang, J., Li, T., Pu, R., Xu, J., Dai, K. "Experimental Investigation on Cyclic Performance of Rotation-Based Metallic Damper", Structural Control and Health Monitoring, 2024(1), 5768511, 2024. https://doi.org/10.1155/2024/5768511

[40] Chan, R. W. K., Albermani, F. "Experimental study of steel slit damper for passive energy dissipation", Engineering Structures, 30(4), pp. 1058–1066, 2008. https://doi.org/10.1016/j.engstruct.2007.07.005

[41] Quan, C., Wang, W., Li, Y., Lu, Z. "Cyclic behaviour of demountable metallic corrugated shear panel dampers", Journal of Building Engineering, 61, 105228, 2022. https://doi.org/10.1016/j.jobe.2022.105228

[42] Teruna, D. R., Majid, T. A., Budiono, B. "Experimental Study of Hysteretic Steel Damper for Energy Dissipation Capacity", Advances in Civil Engineering, 2015, 631726, 2015. https://doi.org/10.1155/2015/631726